



HAL
open science

Unravelling ammonia adsorption mechanisms of adsorbents in humid conditions

Y. Khabzina, D. Farrusseng

► **To cite this version:**

Y. Khabzina, D. Farrusseng. Unravelling ammonia adsorption mechanisms of adsorbents in humid conditions. *Microporous and Mesoporous Materials*, 2018, 265, pp.143-148. 10.1016/j.micromeso.2018.02.011 . hal-01839920

HAL Id: hal-01839920

<https://hal.science/hal-01839920>

Submitted on 27 Mar 2019

HAL is a multi-disciplinary open access archive for the deposit and dissemination of scientific research documents, whether they are published or not. The documents may come from teaching and research institutions in France or abroad, or from public or private research centers.

L'archive ouverte pluridisciplinaire **HAL**, est destinée au dépôt et à la diffusion de documents scientifiques de niveau recherche, publiés ou non, émanant des établissements d'enseignement et de recherche français ou étrangers, des laboratoires publics ou privés.

16 mostly follows the Henry law of ammonia solubilization in water. At the exception of Copper based
17 MOF, the ammonia capture is mostly correlated with the amount of “condensed water” in the
18 micropore. We also generally observe a systematic higher uptake than the Henry law which can be
19 attributed to the effect of confinement i.e surface-condensed phase interaction.

20
21 Ammonia adsorption, screening, MOFs, water adsorption

22 **1. Introduction**

23 Metal-Organic Frameworks (MOFs) are new porous compounds that came to the forefront
24 in the early 2000s. These inorganic-organic hybrid materials exhibit regular pores ranging
25 from micro- to mesopores whose surface can be functionalized by various moieties[1][2][3].
26 Some MOFs have shown very distinct adsorption and storage properties that set them apart
27 from other classic commercial adsorbents, i.e., zeolites and carbons[4][5][6]. Today, we can
28 acknowledge two commercial applications that use a MOF as the adsorbent[7]. Ammonia
29 belongs to the class of toxic industrial components (TICs); it is produced worldwide in an
30 amount of 219 million tons/year[8]. At a concentration of 500 ppm for an exposure time of
31 30 min, it causes irreversible effects, while at a concentration of 3400 ppm, it is lethal within
32 60 minutes. Beyond possible ammonia tank attacks in the event of conflicts[9], ammonia is
33 identified as one of the high-risk chemicals used in manufacturing facilities. The presence of
34 ammonia in the air requires the use of appropriate and efficient protective equipment such as
35 gas masks equipped with type K filter cartridges. Commercial type K cartridges typically
36 contain impregnated activated charcoal with sulphuric or phosphoric acid or transition metals
37 that react with NH_3 [10]. Although this type of adsorbent is efficient in humid conditions, its
38 performance usually degrades in dry conditions[11]. The mechanism of NH_3 adsorption on a

39 carbon-based adsorbent in humid conditions is still unclear. It has been proposed that NH_3 is
40 dissolved in water, which then condenses in the pores of the adsorbent[11][12][13]. To the
41 best of our knowledge, however, no scientific report yet supports this assumption. On the
42 other hand, zeolites perform well in dry conditions but their performance is jeopardised under
43 humid conditions[7]. In contrast, a diverse group of MOFs have shown high NH_3 adsorption
44 capacity under dry and also humid conditions, such as CuBTC[13][14][15], MOF-74[7],
45 FeBTC[16] and Zr-based MOFs[17]. Based on adsorption simulations at the molecular scale,
46 Snurr[18] and co-workers have suggested that the most appropriate adsorbent should be
47 hydrophobic in order to favour NH_3 adsorption versus that of H_2O . It appears obvious that (i)
48 the role of humidity and possible water pore filling (film formation or “condensation”) in the
49 pores of the adsorbent is of key importance and (ii) that different NH_3 adsorption mechanisms
50 co-exist depending on the material’s physico-chemical features. It is impossible, however, to
51 get a clear picture of the performances of different classes of adsorbents because they were
52 not measured in a consistent way, thereby preventing any quantitative comparison. Also,
53 water adsorption is usually not reported at the same conditions for which ammonia adsorption
54 is recorded, which does not enable consistent adsorption mechanism hypotheses to be drawn
55 in humid conditions.

56 This study aims to unravel possible ammonia uptake mechanisms, especially under humid
57 conditions. In order to obtain comprehensive, quantitative trends, ammonia adsorption and
58 co-adsorption under humid conditions have been measured using dynamic breakthrough
59 experiments on a diverse set of adsorbents including zeolites, carbon molecular sieves,
60 carbon and MOFs.

2. Experimental

2.1. Materials

The adsorbents were chosen to cover a wide variety of physico-chemical features, such as composition, pore size, surface functionalisation, etc. For MOFs, metals of several natures were considered: Zr, Ni, Zn, Fe, Cu and Al. Also, MOFs with functional groups such as -NH_2 and -COOH were studied, while for zeolites different structures and Si/Al ratios were selected. In order to benchmark the screened adsorbents, a commercial type K adsorbent from 3M was purchased[19] and tested in the same conditions. It is composed of hard black granules of 850-1700 μm size. All materials were pressed into pellets, crushed and sieved between 425 μm and 600 μm .

UiO-66 type MOFs

Thanks to their thermal, chemical and mechanical stability and also their ability to be functionalised, UiO-66 type solids have attracted considerable interest, especially for NH_3 air purification[10][17][20][21][22]. UiO-66 is made with very stable inorganic bricks $[\text{Zr}_6\text{O}_4(\text{OH})_4]$ that are ideally bonded to twelve 1,4-benzenedicarboxylic acid (BDC) ligands (each Zr atom is 8-coordinated) leading to a micropore of 6 Å and 8 Å diameter. UiO-66-fumarate has tetrahedral cavities of 5 Å in diameter and a 7 Å octahedral cavity[23]. Functionalized UiO-66 such as UiO-66- NH_2 and UiO-66- COOH are prepared with 2-aminoterephthalic acid and 1,2,4-benzenetricarboxylic acid, respectively, instead of BDC. The UiO-66- COOH was obtained following the green synthesis recipe of Reinsh[24]. UiO-66, UiO-66- NH_2 , UiO-66-fumarate were prepared by spray drying following the protocol

84 described in Carné-Sánchez et al.[25] and supplied by ICN2 in the framework of the EC
85 program PRODIA.

86 **CPO-27 type MOFs**

87 Due to their penta-coordinated open metal sites, Ni-CPO-27 and Zn-CPO-27 were
88 selected for this study. CPO-27 is a 1D microporous hexagonal channel structure with
89 calibrated pores of 12 Å[26]. Ni-CPO-27 was obtained from JM[16] and Zn-CPO-27 was
90 supplied by University of St Andrews (USTAN) in the framework of the EC program
91 PRODIA.

92 **Fe-BTC**

93 The structure of Fe-BTC is composed of trimers of iron octahedra sharing a common
94 vertex μ_3 -O linked by benzene-1,3,5-tricarboxylate moieties, leading to two types of
95 mesoporous cages with free apertures of 25 and 29 Å, accessible through microporous
96 windows of 5.5 and 8.6 Å[27]. Fe-BTC was obtained from JM[16].

97 **Cu-BTC**

98 Cu-BTC is composed of dimeric cupric carboxylate units that are connected with benzene-
99 1,3,5-tricarboxylate to form a three-dimensional face-centred cubic crystal. The larger pores
100 correspond to a square cross-section of approximately 9 Å in diameter, while the smaller
101 pores correspond to a tetrahedral side pocket of approximately 5 Å in diameter[28]. It
102 possesses coordinatively unsaturated metal sites (CUS) which can be responsible of the
103 reactivity of Cu with NH₃[29]. CuBTC was supplied by MOF Technologies.

104 **Al-MIL-101-NH₂**

105 Al-MIL-101-NH₂ possesses Al³⁺ coordinatively unsaturated metal sites (CUS), allowing
106 its use as a mild Lewis acid[30]. The solid exhibits two types of quasi-spherical mesoporous
107 cages formed by 12 pentagonal and 16 faces, respectively. The so-called medium cavities are

108 accessible through 12 Å pentagonal windows, while the large cavities are communicated
109 through the same pentagonal windows and 16 Å hexagonal windows[31]. AI-MIL-101-NH₂
110 was synthesized using the protocol described in Hartmann et al.[32].

111 **Zeolites**

112 Sodium-form zeolites ZSM-5, Beta and faujasites were supplied by Zeolyst International.
113 ZSM-5, an MFI-type zeolite, is composed of a three-dimensional network pore system with
114 straight, parallel channels intersected by zigzag channels and with 10-membered rings of
115 oxygen atoms controlling the entrance to the channels[33]. This zeolite type has a medium
116 pore size of approximately 5.3 Å[33]. Faujasite-type structures are constructed from sodalite
117 cages connected by six-membered ring pores. Spherical supercages, 11.2 Å in diameter,
118 reside between the sodalite cages and are connected by 12-MR pores of size 7.4 Å x 7.4
119 Å[34]. Like faujasites, Beta zeolite has a three-dimensional, interconnected 12-MR pore
120 system; the dimensions of its largest pores are 6.6 Å x 6.7 Å[34].

121 **Carbon molecular sieves**

122 The Carboxen 564 and Carbosieve G 60/80 were purchased from Sigma Aldrich. These
123 carbon molecular sieves have a pore size from 6 to 15 Å.

124 *2.2. Experimental set-up*

125 The study of ammonia adsorption was carried out by breakthrough measurements. A flow
126 of 100 mL/min containing 1200 ppm ammonia in the gas phase was passed through a 0.4 cm
127 height adsorbent packed into a 7 mm i.d. fritted glass tube (0.15 cm³). Prior to the
128 breakthrough experiments, the adsorbents were first evacuated at 150°C for MOFs and 250°C
129 for zeolites, under 100 mL/min N₂, for 30 minutes. This technique provides a quantitative
130 evaluation of the uptake capacities of ammonia in dry or humid conditions. The experimental

set-up is shown in Figure 1. Breakthrough measurements were conducted at ambient temperature, under dry and humid conditions. Humid conditions were generated by humidifying a controlled flow of N_2 to obtain a relative humidity of 40% for the stream. For measurements in humid conditions, the adsorbents were wetted by equilibration at the testing relative humidity of 40% prior to feeding the humidified ammonia stream by the same RH. Outlet flow analysis was performed online by infrared spectroscopy. The breakthrough curves were plotted as a function of time without normalisation per unit mass (x-axis) nor per initial concentration (C_0) (y-axis). The adsorption capacities of ammonia and water were evaluated by integrating the resulting breakthrough curves until the concentration $C(t)$ reached the inlet concentration (C_0) [7]. The total NH_3 and water capacities were calculated on the basis of adsorbent mass.

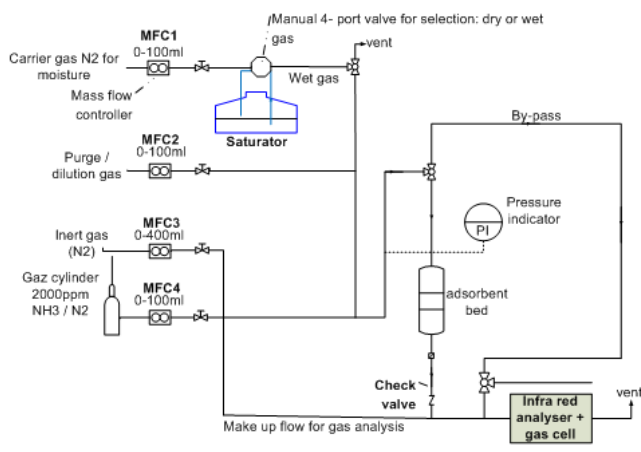


Figure 1. Experimental set-up scheme

3. Results and discussion

The breakthrough curves of the MOF adsorbents are presented here, for purposes of illustration, in Figures 2 through 5. All other breakthrough curves can be found in the SI. For

the sake of readability, the results are plotted in different figures for dry and humid conditions: UiO-type MOFs in Figures 2 and 3, and other MOFs in Figures 4 and 5.

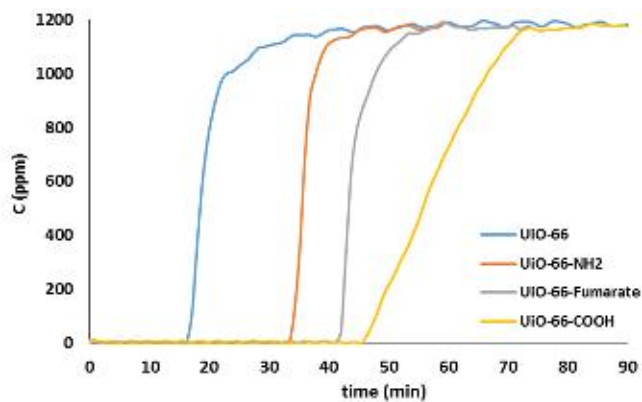


Figure 2. Ammonia breakthrough curves of UiO type MOFs in dry condition.

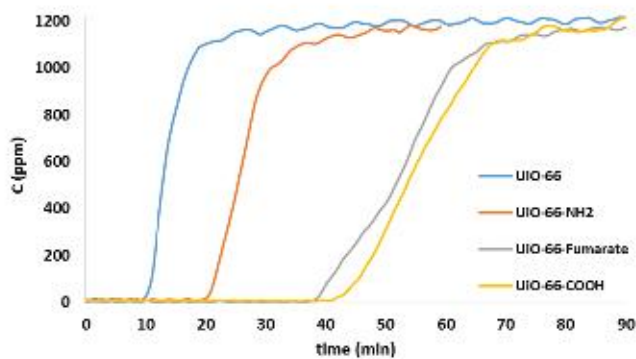


Figure 3. Ammonia breakthrough curves of UiO type MOF in humid condition.

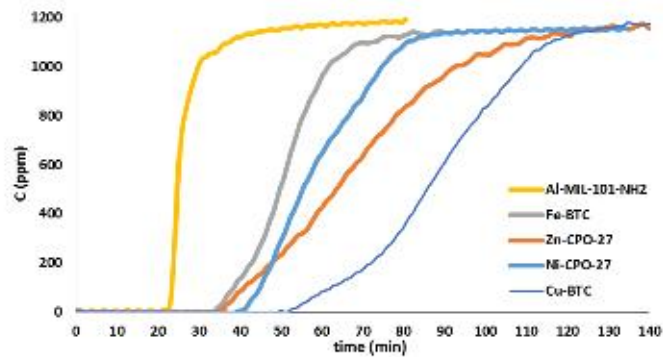


Figure 4. Ammonia breakthrough curves of various MOFs in dry condition.

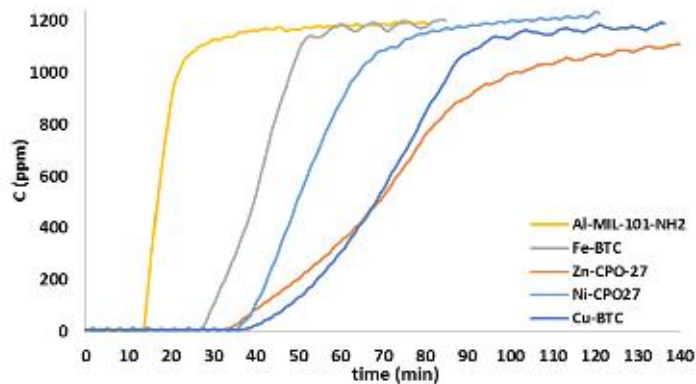


Figure 5. Ammonia breakthrough curves of various MOFs in humid condition.

Apart from different breakthrough times, we can observe different curve profiles. For some adsorbents, the concentration increases promptly after NH_3 breaks, whereas for others, the concentration increases slowly. These observations were also reported by Glover et al.[7] for a series of CPO-27. In addition, we can see that for a particular adsorbent the profiles are very similar in both dry and humid conditions, with the exception of UiO-66-fumarate. For

188 UiO-66, UiO-66-NH₂ and Al-MIL-101-NH₂, the slope is steep, whereas for others the NH₃
189 concentration increases slowly until the saturation. Although we cannot rule out the effect of
190 water condensation effect under humid conditions, the rate at which the concentration
191 evolves is usually linked to the regime at which the uptake occurs, i.e., chemical or mass
192 transport controlled regimes. For steep profiles there is obviously no mass transport limitation
193 (ex. Al-MIL-101-NH₂), whereas for smooth profiles we can assume that internal mass
194 transport limitation may occur (such as for Zn-CPO-27)[21]. We can rule out different
195 packing or grain size, since all samples were sieved within a narrow fraction size range of
196 425-600 μm. The difference in breakthrough profiles may possibly arise from different grain
197 density (i.e macroporosity) after tableting, which is MOF-dependent[35]. We can assume
198 that very densely-packed crystallites may penalise the transport rate in the grains.

199
200 When comparing the NH₃ uptake data obtained here with data reported elsewhere, we can
201 observe good agreement in some cases and major apparent inconsistencies in other cases (see
202 table S1 in the SI). Regarding matching measurements, we can cite uptakes for Fe-BTC and
203 Ni-CPO-27 (40 and 58 mg/g), which are similar to those obtained by Hindocha et al.[16] (47
204 and 64 mg/g), keeping in mind that the solids were shaped and tested under slightly different
205 yet comparable conditions. We recall that the Ni-CPO-27 and Fe-BTC solids tested here were
206 supplied by Johnson Matthey[16] in the context of the “PRODIA” EC program for crossed
207 validation purposes. The sample being the same, it is not surprising to find consistent results.
208 We also see for Zn-CPO-27 very good agreement with the result obtained by Glover et al.[7]:
209 49 mg/g versus 48 mg/g. A fair matching result is also observed for Cu-BTC provided here
210 by MOFTech and that of Hindocha[16] study (112 mg/g, 105 mg/g). On the other hand, we
211 can acknowledge rather systematic inconsistencies for uptakes on UiO-66 type materials. We

212 note that the preparation methods used here for UiO-66 type materials are very different from
213 methods reported elsewhere. UiO-66 and UiO-66-NH₂ were obtained by direct synthesis in a
214 spray-dryer, whereas they were prepared using conventional batch processes in the relevant
215 literature[17][21][20]. Also, UiO-66-COOH was prepared in water here, rather than in DMF
216 as for Joshi et al.[22]. It is now well acknowledged that for UiO-type solids the synthesis
217 processes and parameters have a major impact on the nature and concentration of structural
218 defects. Lillerud et al.[36] have shown that the synthesis temperature and the use of
219 modulators strongly modify the stability and porous structure of UiO-66 solids. It has been
220 further shown that UiO-66 solids prepared under different conditions exhibit different water
221 adsorption profiles³⁸. From this literature analysis, we can conclude that although powder
222 XRD and surface area data can be considered as fingerprints of the “quality” of the synthesis,
223 there are insufficient for revealing the potential performances in NH₃ capture from air and
224 conversely that the synthesis processes and parameters are key aspects, possibly as important
225 as the selection of an ideal MOF design itself.

226 In our study, water breakthrough measurements at RH =40% (breakthrough curves are
227 reported in the SI) were carried out systematically prior to NH₃ feeding; the water uptake
228 amounts are reported in Table 1. The comparison of water uptake values with data from the
229 literature is not straightforward, because the values reported usually correspond to 100% RH,
230 and different values are reported for the same solids using isotherm-type
231 measurements[6][37]. For Ni-CPO-27, Zn-CPO-27 and UiO-66-COOH, we can observe
232 major deviations in water uptake measured by breakthrough measurements as compared to
233 literature data. For Ni-CPO-27 and Zn-CPO-27, we found 0.31 and 0.33 g/g respectively
234 versus 0.11 and 0.24 for Glover et al.[7] at 50% RH. In the case of UiO-66-COOH, we
235 measured a water uptake of 0.25 g/g at 40% RH versus 0.045 g/g at 40% for Joshi et al.[22].

236 These discrepancies point toward differences in the surface and/or porous structural features
237 resulting from different synthesis routes. In fact, water adsorption is a very sensitive probe
238 for the measurement of structural defects and has recently been proposed as a characterization
239 approach for probing the defect concentration of UiO-66 MOF[38]. Discussion about the
240 nature of these defects is beyond the scope of this paper, and proposals can be found
241 elsewhere³⁸. Nevertheless, at the light of this discussion on the impact of surface defects, it
242 is not surprising to observe different ammonia capacity data on solids which have been
243 prepared by other methods.

244
245 We note that carbon molecular sieves are rather hydrophobic, with uptakes lower than 0.1
246 g/g, in contrast to the commercial carbon based adsorbent (3M) which shows a large water
247 uptake.

248
249 The main underlying mechanism of ammonia uptake in humid conditions is revealed when
250 the ammonia uptake is plotted as a function of the water uptake at 40% RH (c.f. Figure 6).
251 Except for a few cases discussed below, we observe that the experimental points seem to
252 follow a linear trend. Hence, this indicates that the ammonia uptake is determined mainly by
253 the amount of water that is adsorbed in the adsorbent, suggesting a solubilisation-like
254 mechanism. The solubility of NH₃ in water as a function of NH₃ pressure, assuming
255 undissociation of NH₃, corresponds to the well-known Henry's law. We plotted the straight
256 line corresponding to solubilized NH₃ amount as a function of the volume of adsorbed water,
257 using a solubility of 142.8 mgNH₃/gH₂O which corresponds to the Henry constant of 70
258 mol.g⁻¹.bar⁻¹ (NIST)[39] and an NH₃ pressure of 0.12 bar (corresponding to 1200 ppm).
259 Although there are deviations, it is obvious that the linear trend very much corresponds to

Henry's law, thereby pointing to a solubilisation-like mechanism. We can propose three hypotheses that may explain the observed deviations from Henry's law. Firstly, there could be experimental errors on the amount of adsorbed water because of the high temperature sensitivity of the relative humidity. Nevertheless, we can see a general bias i.e. Henry's law underestimates most experimental data. At this stage we can question whether the Henry's law hypotheses are fulfilled. First, we shall determine whether the pores are partially or completely filled with water at 40% RH. In an earlier study, we defined the critical relative humidity value at which half of the micropore volume is filled (alpha value).

Table 1. Summarized table of ammonia and water adsorption capacities.

Adsorbent	BET surface area (m ² /g)	Ammonia adsorption amount at 1200 ppm (mg/g)		Water adsorption amount at 0.4 RH (g/g)	Alpha value
		Dry	Wet		
UiO-66	1120	23	26	0.11	0.30[40]
UiO66-NH₂	625	24	33	0.21	0.15[40]
UiO66-fumarate	512	42	32	0.28	0.10[23]
UiO66-COOH	614	54	54	0.25	0.2 [#]
Ni-CPO-27	855	55	58	0.31	0.02[23]
Zn-CPO-27	373	47	49	0.33	<0.15[7]
Fe-BTC	1176	34	40	0.24	0.38[41]
Cu-BTC	1541	91	112	0.29	0.10[42]
Al-MIL-101-NH₂	3000	29	39	0.18	0.35[43]
ZSM-5 (Si/Al : 23)	384	38	25	0.13	n.d
Y (Si/Al : 14.3)	696	7	7	0.02	n.d
Y (Si/Al : 5.5)	710	31	12	0.16	n.d
Beta	549	24	24	0.14	n.d
Carboxen 564	400	0.79	2	0.02	0.70[44]
Carbosieve G	1160	10	13	0.09	>0.8[44]
Type K Adsorbent	810	39	56	0.36	n.d.

this study

271 For MOFs that exhibit a Type V isotherm profile (S-shape) it corresponds approximately
272 to the inflection point of the isotherm. Except for the carbon molecular sieve, we can note
273 that in our case, applied relative humidity of $p/p^{\circ}=0.4$ is higher than the alpha value of the
274 adsorbents, meaning that at least 50% of the micropore volume of the tested adsorbents is
275 filled by water. On another note Henry's law supposes that the water is a bulk macroscopic
276 phase. The physical properties of "water" in micropore shall be addressed. Indeed the
277 arrangement of water molecules should be more similar to a multilayer of water molecules
278 on the surface of an adsorbent, thus departing from a pure water phase. In the recent literature
279 on zeolites, mesoporous silicates and MOFs, Ho et al.[45] have reported similar over
280 solubility effects of gases when the "liquids" are confined in nanoporous materials.
281 According to this study, the higher solubility of gases observed can arise either from an
282 increased solubility due to a layering effect of the "liquid" phase or from higher adsorption
283 at the solid-"liquid" interface. Although uptake mostly follow the Henry law, we propose that
284 the solid surface play a major role in the adsorption mechanisms. The elucidation of
285 molecular interactions at the surface of the different solids is beyond the scope of this study.

286 We wish to point out that the assumption of the solubilisation-like mechanism holds not
287 only for the adsorbents tested in this study but also for series of UiO-66 and CPO-27
288 adsorbents tested elsewhere (see Figure 6, blue and purple dots)[22][7]. As we underlined
289 above, physical properties of MOFs, especially the UiO-66 type, can depend on synthesis
290 processes and parameters. Despite the nature and concentration of defects, we can see that
291 the solubility mechanism assumption remains valid. As a consequence, it is possible to
292 estimate the ammonia adsorption capacity from water uptake data regardless the nature of
293 the porous adsorbents and their synthesis method.
294

295 We note, however, that two cases strongly depart from Henry's law. Obviously, NH₃
296 uptakes on CuBTC and UiO-66-(COOCu)₂ outweigh the solubility hypothesis. For CuBTC,
297 as cited in Peterson et al. paper[14], NH₃ reacts with the solid to produce Cu hydroxide and
298 (NH₄)₃BTC species which is accompanied with the collapse of the microporous structure.
299 From Peterson conclusions on the reactivity of CuBTC with ammonia, we can suppose here
300 the reaction of 2 ammonia per BTC. Hence we can propose that for CuBTC, chemisorption
301 (or reactivity) occurs in humid conditions instead of physisorption. The mechanisms of
302 interactions between CuBTC and NH₃ in dry and humid conditions have been studied in
303 details and can be found elsewhere[14][29].

304 For data on UiO-66-(COOCu)₂[22], we find a 1.1 relation for NH₃:Cu assuming an ideal
305 composition of the adsorbent which points toward a chemisorption/reactivity mechanism.
306 Although the adsorption capacities of the Cu-containing MOF are well above other
307 adsorbents tested here, their assessment for a commercial solution is out of scope of this study
308 since there are numbers of other criteria to be fulfilled[16].
309

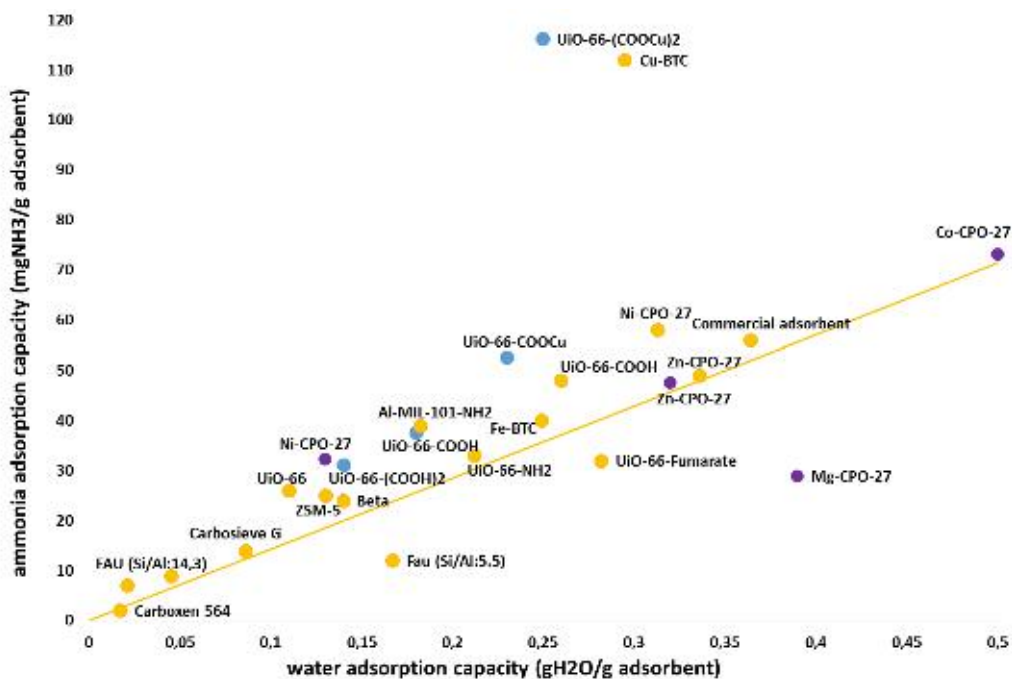


Figure 6. Ammonia uptake as a function of water uptake measured by breakthrough experiments at 40% RH and 20°C for a NH₃ challenge concentration of 1200 ppm (yellow). Additional data from the literature are added: Glover et al.[7] (purple, 1294 ppm NH₃) and Joshi et al.[22] (blue, 1431 ppm NH₃). The straight line corresponds to the amount of NH₃ solubilized in water according to Henry's law with $k^{\circ}H = 70$ mol/kg/bar at 25°C (NIST).

In a recent study, Moghadam et al.[46] conclude from a large hypothetical screening of MOF structures that theoretical simulations show that strongly hydrophilic MOFs present highly competitive water adsorption and therefore exhibit poor selectivity towards NH₃. This conclusion goes against the experimental facts presented here. Indeed, we have clearly established, based on the screening of a diverse adsorbent library that a linear trend is observed between water uptake and ammonia uptake. While the study of solid-gas

327 interactions remains relevant, the bias of the study of Moghadam et al.[46] likely arises from
328 the assumption that water is not present in “condensed” states for the NH₃ uptake simulation.

329 **4. Conclusion**

330 Generally speaking, the uptake mechanisms of ammonia in microporous solids for air
331 purification can be classified in three main groups that may co-exist: (i) solubilisation, (ii)
332 physisorption and (iii) chemisorption. We show that ammonia uptake mainly follow the
333 Henry law suggesting a solubilisation-like mechanism which occurs when water condenses
334 in the pore, i.e., at larger RH than the alpha value. We underline the effect of surface
335 interactions (i.e confinement) which might be responsible for the higher uptake when
336 comparing to the Henry law in water bulk phase. On practical aspects, it becomes possible to
337 estimate the ammonia adsorption capacity from water uptake data regardless the nature of
338 microporous solids or its synthesis method.

339 For adsorbents that are made or impregnated with reactive species such as Cu²⁺ species,
340 chemisorption occurs to yield complexes or basic-acid adducts in a ratio close to 1:1. In
341 addition to high uptake in the case of Cu²⁺ complexes, this mechanism offers stronger
342 ammonia fixation, which can be an asset for K type protection filter.

343 **Acknowledgements**

344 This work has been carried out within the ProDIA project that has received funding
345 from the European Union's Horizon 2020 research and innovation program under grant
346 agreement No. 685727. The authors would like to thank Johnson Matthey, University of St

Andrews, MOF Technologies and the Catalan Institute of Nanoscience and Nanotechnology
for supplying samples.

References

- [1] D. Farrusseng, *Metal-Organic Frameworks : Applications from Catalysis to Gas Storage*, Wiley-VCH, 2011.
- [2] S. Kaskel, *The Chemistry of Metal-Organic Frameworks : Synthesis, Characterization, and Applications.*, Wiley, 2016.
- [3] H. Deng, C.J. Doonan, H. Furukawa, R.B. Ferreira, J. Towne, C.B. Knobler, B. Wang, O.M. Yaghi, *Science* 327 (2010) 846–850.
- [4] J.A. Mason, M. Veenstra, J.R. Long, H.-C. Zhou, H. Leclerc, A. Ghoufi, P. Bazin, A. Vimont, M. Daturi, T. Devic, C. Serre, G.D. Weireld, G. Maurin, Y. Han, Z. Shi, S. Feng, J. Li, *Chem. Sci.* 5 (2014) 32–51.
- [5] H.-C. Zhou, Y. Liu, Z.U. Wang, *Greenh. Gas Sci Technol* 2 (2012) 239–259.
- [6] M.F. de Lange, K.J.F.M. Verouden, T.J.H. Vlught, J. Gascon, F. Kapteijn, *Chem. Rev.* 115 (2015) 12205–12250.
- [7] T. Grant Glover, G.W. Peterson, B.J. Schindler, D. Britt, O. Yaghi, *Chem. Eng. Sci.* 66 (2011) 163–170.
- [8] <http://www.societechimiquedefrance.fr/extras/Donnees/mine/nh3/texnh3.htm>.
- [9] T.W. Karasik, *Toxic Warfare*, Santa Monica, 2002.
- [10] K.-D. Henning, S. Schäfer, *Gas Sep. Purif.* 7 (1993) 235–240.
- [11] P. Lodewyckx, *Interface Sci. Technol.* 7 (2006) 475–528.
- [12] M. Gonçalves, L. Sánchez-García, E. de Oliveira Jardim, J. Silvestre-Albero, F. Rodríguez-Reinoso, *Environ. Sci. Technol.* 45 (2011) 10605–10610.
- [13] C. Petit, B. Mendoza, T.J. Bandoz, *Langmuir* 26 (2010) 15302–15309.
- [14] G.W. Peterson, G.W. Wagner, A. Balboa, J. Mahle, T. Sewell, C.J. Karwacki, *J. Phys. Chem. C* 113 (2009) 13906–13917.
- [15] T. Watanabe, D.S. Sholl, *J. Chem. Phys.* 133 (2010) 94509.
- [16] S. Hindocha, S. Poulston, *Faraday Discuss.* 201 (2017) 113–125.
- [17] H. Jasuja, G.W. Peterson, J.B. Decoste, M.A. Browe, K.S. Walton, *Chem. Eng. Sci.* 124 (2015) 118–124.
- [18] K.C. Kim, D. Yu, R.Q. Snurr, *Langmuir* 29 (2013) 1446–1456.
- [19] <https://www.amazon.co.uk/3M-A26118-6054-K1-Filter/dp/B000U6Y1P4>.
- [20] W.P. Mounfield, M. Taborga Claire, P.K. Agrawal, C.W. Jones, K.S. Walton, *Ind. Eng. Chem. Res.* 55 (2016) 6492–6500.
- [21] G.W. Peterson, J.B. DeCoste, F. Fatollahi-Fard, D.K. Britt, *Ind. Eng. Chem. Res.* 53 (2014) 701–707.

- 374 [22] J.N. Joshi, E.Y. Garcia-Gutierrez, C.M. Moran, J.I. Deneff, K.S. Walton, *J. Phys. Chem. C* 121 (2017) 3310–3319.
- 375 [23] H. Furukawa, F. Gándara, Y.-B. Zhang, J. Jiang, W.L. Queen, M.R. Hudson, O.M. Yaghi, *J. Am. Chem. Soc.* 136 (2014) 4369–
376 4381.
- 377 [24] H. Reinsch, *Eur. J. Inorg. Chem.* 2016 (2016) 4290–4299.
- 378 [25] A. Carné-Sánchez, I. Imaz, M. Cano-Sarabia, D. Maspocho, *Nat. Chem.* 5 (2013) 203–11.
- 379 [26] S. Cadot, L. Veyre, D. Luneau, D. Farrusseng, E. Alessandra Quadrelli, *J. Mater. Chem. A* 2 (2014) 17757–17763.
- 380 [27] A. Dhakshinamoorthy, M. Alvaro, H. Garcia, *Adv. Synth. Catal.* 352 (2010) 711–717.
- 381 [28] H. Yang, S. Orefuwa, A. Goudy, *Microporous Mesoporous Mater.* 143 (2011) 37–45.
- 382 [29] N. Nijem, K. Fürsich, H. Bluhm, S.R. Leone, M.K. Gilles, *J. Phys. Chem. C* 119 (2015) 24781–24788.
- 383 [30] A. Henschel, K. Gedrich, R. Kraehnert, S. Kaskel, *Chem. Commun.* (2008) 4192–4194.
- 384 [31] P. Serra-Crespo, E. V Ramos-Fernandez, J. Gascon, F. Kapteijn, *Chem. Mater.* 23 (2011) 2565–2572.
- 385 [32] M. Hartmann, M. Fischer, *Microporous Mesoporous Mater.* 164 (2012) 38–43.
- 386 [33] E. Beersden, D. Dubbeldam, B. Smit, T.J.H. Vlugt, S. Calero, *J. Phys. Chem. B* 107 (2003) 12088–12096.
- 387 [34] J.E. Krohn, M. Tsapatsis, *Langmuir* 22 (2006) 9350–9356.
- 388 [35] J. Dhainaut, C. Avci-Camur, J. Troyano, A. Legrand, J. Canivet, I. Imaz, D. Maspocho, H. Reinsch, D. Farrusseng,
389 *CrystEngComm* 19 (2017) 4211–4218.
- 390 [36] G.C. Shearer, S. Chavan, J. Ethiraj, J.G. Vitollo, S. Svelle, U. Olsbye, C. Lamberti, S. Bordiga, K.P. Lillerud, *Chem. Mater.* 26
391 (2014) 4068–4071.
- 392 [37] J. Canivet, A. Fateeva, Y. Guo, B. Coasne, D. Farrusseng, H. Na, C. Liu, F. Sun, G. Zhu, H. Tokoro, S. -i. Ohkoshi, M.
393 Verdagner, A. Cabeza, C. Riekkel, G. Férey, C. Serre, *Chem. Soc. Rev.* 43 (2014) 5594–5617.
- 394 [38] S. Dissegna, R. Hardian, K. Epp, G. Kieslich, M.-V. Coulet, P. Llewellyn, R.A. Fischer, 19 (2017) 4035–4228.
- 395 [39] T.K. Sherwood, *Ind. Eng. Chem.* 17 (1925) 745–747.
- 396 [40] J. Canivet, J. Bonnefoy, C. Daniel, A. Legrand, B. Coasne, D. Farrusseng, R.Q. Snurr, G. Férey, F. Kapteijn, M. Latroche, *New
397 J. Chem.* 38 (2014) 3102–3111.
- 398 [41] Y.-K. Seo, J.W. Yoon, J.S. Lee, Y.K. Hwang, C.-H. Jun, J.-S. Chang, S. Wuttke, P. Bazin, A. Vimont, M. Daturi, S. Bourrelly,
399 P.L. Llewellyn, P. Horcajada, C. Serre, G. Férey, *Adv. Mater.* 24 (2012) 806–810.
- 400 [42] Y. Cai, Y. Zhang, Y. Huang, S.R. Marder, K.S. Walton, *Cryst. Growth Des.* 12 (2012) 3709–3713.
- 401 [43] T. Wittmann, R. Siegel, N. Reimer, W. Milius, N. Stock, J. Senker, *Chem. - A Eur. J.* 21 (2015) 314–323.
- 402 [44] V. Detlev, Helmig Lee, *Anal. Chem.* 67 (1995) 4380–4386.
- 403 [45] L.N. Ho, Y. Schuurman, D. Farrusseng, B. Coasne, *J. Phys. Chem. C* 119 (2015) 21547–21554.

- 404 [46] P.Z. Moghadam, D. Fairen-Jimenez, R.Q. Snurr, M.A. Browe, K.S. Walton, Z.R. Herm, T.-H. Bae, J.R. Long, M. Lanuza, D.B.
405 Galloway, J.J. Low, R.R. Willis, R.Q. Snurr, J.F. Stoddart, N. Planas, K. Lee, T. Pascal, L.F. Wan, D. Prendergast, J.B. Neaton,
406 B. Smit, J.B. Kortright, L. Gagliardi, S. Bordiga, J.A. Reimer, J.R. Long, *J. Mater. Chem. A* 4 (2016) 529–536.

407